

Supplementary Information

Facile Synthesis and Phase Stability of Cu-based $\text{Na}_2\text{Cu}(\text{SO}_4)_2 \cdot x\text{H}_2\text{O}$ ($x = 0-2$) Sulfate Minerals as Conversion type Battery Electrodes

Shashwat Singh,^{†#} Audric Neveu,[#] K. Jayanthi,^{\$} Tisita Das,[‡] Sudip Chakraborty,[‡]

Alexandra Navrotsky,^{\$} Valérie Pralong,[#] and Prabeer Barpanda^{†§}*

[†] Faraday Materials Laboratory (FaMaL), Materials Research Center, Indian Institute of Science, Bangalore 560012, India

[#] Normandie University, ENSICAEN, UNICAEN, CNRS, CRISMAT, 14000 Caen, France

^{\$} School of Molecular Sciences and Navrotsky Eyring Center for Materials of the Universe, Arizona State University, Tempe, Arizona 85287, United States

[‡] Materials Theory for Energy Scavenging (MATES) Lab, Harish-Chandra Research Institute (HRI), HBNI, Chhatnag Road, Jhansi, Prayagraj 211019, India

[§] Helmholtz Institute Ulm (HIU), Helmholtzstraße, Ulm 89081, Germany

Corresponding Author

*E-mail: prabeer@iisc.ac.in

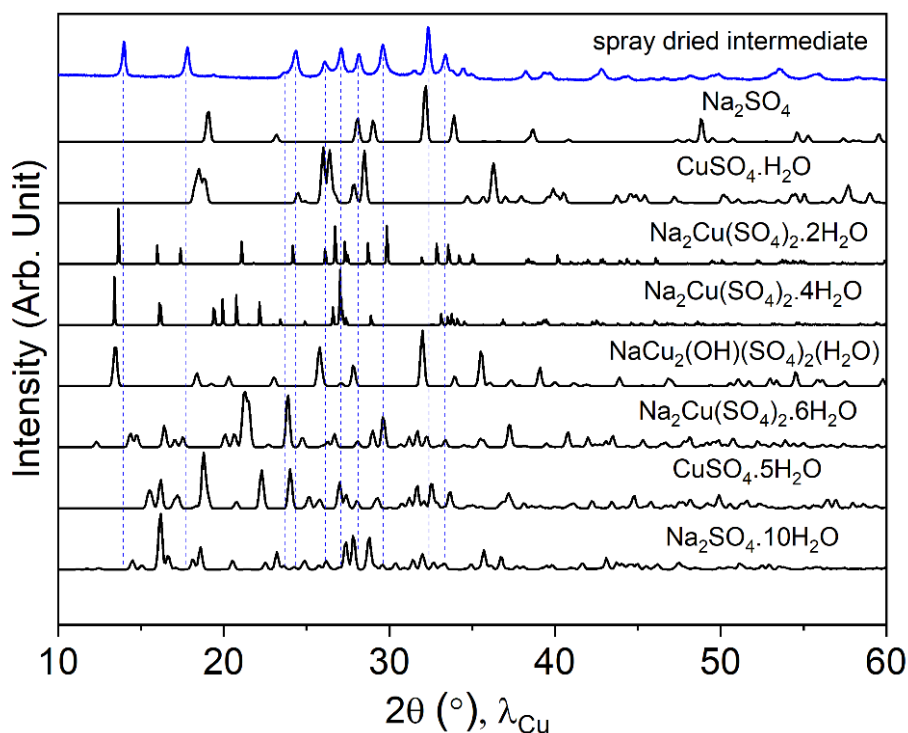


Fig. S1 PXRD pattern of the spray dried intermediate complex powder (blue line) is compared with the reference patterns of hydrated compounds $\text{Na}_2\text{Cu}(\text{SO}_4)_2 \cdot x\text{H}_2\text{O}$ ($x = 2, 4$ and 6), natrochalcite $\text{NaCu}_2(\text{SO}_4)_2(\text{OH}) \cdot \text{H}_2\text{O}$ and precursors $\text{CuSO}_4 \cdot 5\text{H}_2\text{O}$, $\text{CuSO}_4 \cdot \text{H}_2\text{O}$, $\text{Na}_2\text{SO}_4 \cdot 10\text{H}_2\text{O}$ and Na_2SO_4 .

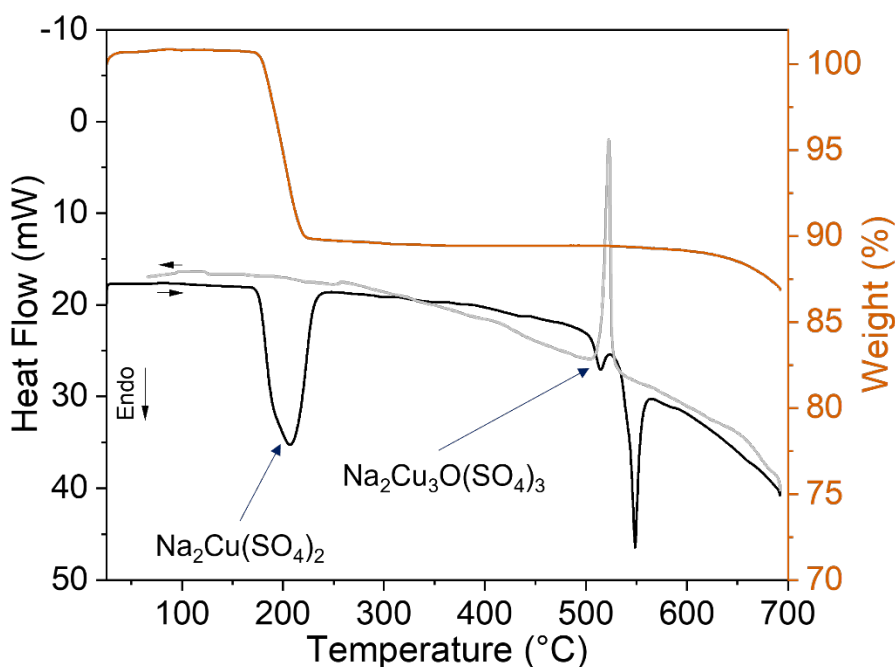


Fig. S2 Simultaneous thermal analysis (thermogravimetric and differential scanning calorimetry) plot for spray dried intermediate complex powder. The data was acquired at a heating rate of $10\text{ }^\circ\text{C}/\text{min}$ in N_2 gas flow ($50\text{ mL}/\text{min}$). The grey line indicates the DSC curve acquired during cooling.

Table S1 Lattice and atomic parameters of kröhnkite $\text{Na}_2\text{Cu}(\text{SO}_4)_2 \cdot 2\text{H}_2\text{O}$ determined from Rietveld refinement.

Formula [Molecular weight]	$\text{Na}_2\text{Cu}(\text{SO}_4)_2 \cdot 2\text{H}_2\text{O}$ [337.68]
Crystal system	Monoclinic
Space group	$P 2_1/c$ (#14), $Z = 2$
Unit cell parameter (Å)	$a = 5.8078(1)$, $b = 12.6664(0)$, $c = 5.5173(4)$ $\beta = 108.44$
Unit cell volume (Å³)	385.02(3)
Theoretical density (gcm⁻³)	2.9128
Reliability factors & goodness of fit values	$R_p = 9.82\%$, $R_{wp} = 8.81\%$, $\chi^2 = 11.3$

Atom	Site	x	y	z	Occupancy	U _{iso}
Na	4e	0.5744	0.1253	0.2109	1	0.0003
Cu	2a	0	0	0	1	0.0003
S	4e	0.2371	0.1198	0.5428	1	0.0003
O1	4e	0.0108	0.1736	0.4907	1	0.0003
O2	4e	0.3004	0.0577	0.7796	1	0.0003
O3	4e	0.2328	0.0481	0.3391	1	0.0003
O4	4e	0.4456	0.1940	0.5635	1	0.0003
O5	4e	0.8374	0.1366	0.9497	1	0.0003
H1	4e	0.8976	0.1859	0.9680	1	0.0003
H2	4e	0.7120	0.1400	0.7900	1	0.0003

Table S2 Lattice and atomic parameters of saranchinaite $\text{Na}_2\text{Cu}(\text{SO}_4)_2$ determined from Rietveld refinement.

Formula [Molecular weight]	$\text{Na}_2\text{Cu}(\text{SO}_4)_2$ [301.65]
Crystal system	Monoclinic
Space group	$P 2_1$ (#4), $Z = 8$
Unit cell parameter (Å)	$a = 8.9672(9)$, $b = 15.5408(0)$, $c = 10.1401(0)$ $\beta = 107.087$
Unit cell volume (Å³)	1350.74
Theoretical density (gcm⁻³)	2.9667
Reliability factors & goodness of fit values	$R_p = 14.3\%$, $R_{wp} = 14.6\%$, $\chi^2 = 21.25$

Atom	Site	x	y	z	Occupancy	U_{iso}
Na1	2a	0.28374	0.42257	0.05243	1	0.0003
Na2	2a	0.28937	0.41204	0.61718	1	0.0003
Na3	2a	0.97519	0.68519	0.24565	1	0.0003
Na4	2a	0.61794	0.54975	0.66348	1	0.0003
Na5	2a	0.36251	0.80324	0.41809	1	0.0004
Na6	2a	0.60322	0.58649	0.08643	1	0.0003
Na7	2a	0.93999	0.72662	0.66951	1	0.0003
Na8	2a	0.62924	0.26826	0.15688	1	0.0002
Cu1	2a	0.65082	0.07897	0.67666	1	0.0002
Cu2	2a	0.92753	0.31663	0.01380	1	0.0001
Cu3	2a	0.90613	0.53165	0.96179	1	0.0002
Cu4	2a	0.90104	0.53194	0.48433	1	0.0002
O1	2a	0.87930	0.05876	0.03320	1	0.0002
O2	2a	0.00950	0.36789	0.23260	1	0.0002
O3	2a	0.96460	0.41646	0.91060	1	0.0002
O4	2a	0.85550	0.64283	0.02120	1	0.0002
O5	2a	0.50010	0.67831	0.38250	1	0.0002
O6	2a	0.84960	0.79062	0.95450	1	0.0002
O7	2a	0.69060	0.50090	0.91580	1	0.0003
O8	2a	0.61240	0.71596	0.93700	1	0.0003
O9	2a	0.88390	0.47591	0.68250	1	0.0003
O10	2a	0.71580	0.67068	0.28010	1	0.0003

O11	2a	0.73580	0.21729	0.37890	1	0.0003
O12	2a	0.74370	0.61348	0.50660	1	0.0002
O13	2a	0.71220	0.34973	0.98610	1	0.0002
O14	2a	0.50910	0.01872	0.74650	1	0.0002
O15	2a	0.21090	0.47467	0.27310	1	0.0002
O16	2a	0.05710	0.45993	0.43170	1	0.0002
O17	2a	0.90050	0.32126	0.71640	1	0.0003
O18	2a	0.94100	0.11454	0.43230	1	0.0002
O19	2a	0.79440	0.14012	0.59220	1	0.0002
O20	2a	0.55720	0.39300	0.75650	1	0.0003
O21	2a	0.13590	0.40572	0.76670	1	0.0003
O22	2a	0.64360	0.13436	0.01570	1	0.0003
O23	2a	0.79190	0.16699	0.85730	1	0.0002
O24	2a	0.76060	0.67814	0.78100	1	0.0003
O25	2a	0.48680	-0.13490	0.73140	1	0.0003
O26	2a	0.88610	0.20960	0.09590	1	0.0002
O27	2a	0.47780	0.42807	0.95780	1	0.0004
O28	2a	0.72610	0.76692	0.46900	1	0.0003
O29	2a	0.46640	-0.05170	0.52530	1	0.0003
O30	2a	0.26130	-0.04830	0.63560	1	0.0003
O31	2a	0.94220	0.51881	0.20350	1	0.0002
O32	2a	0.66990	0.06576	0.38080	1	0.0003
S1	2a	0.56747	0.41358	0.89123	1	0.0001
S2	2a	0.74208	0.71073	0.92625	1	0.0001
S3	2a	0.06562	0.43822	0.30261	1	0.0001
S4	2a	0.66852	0.69608	0.39968	1	0.0001
S5	2a	0.75860	0.14268	0.42532	1	0.0002
S6	2a	0.97682	0.40069	0.74203	1	0.0002
S7	2a	0.42819	-0.06170	0.65153	1	0.0002
S8	2a	0.78464	0.14354	1.00114	1	0.0001

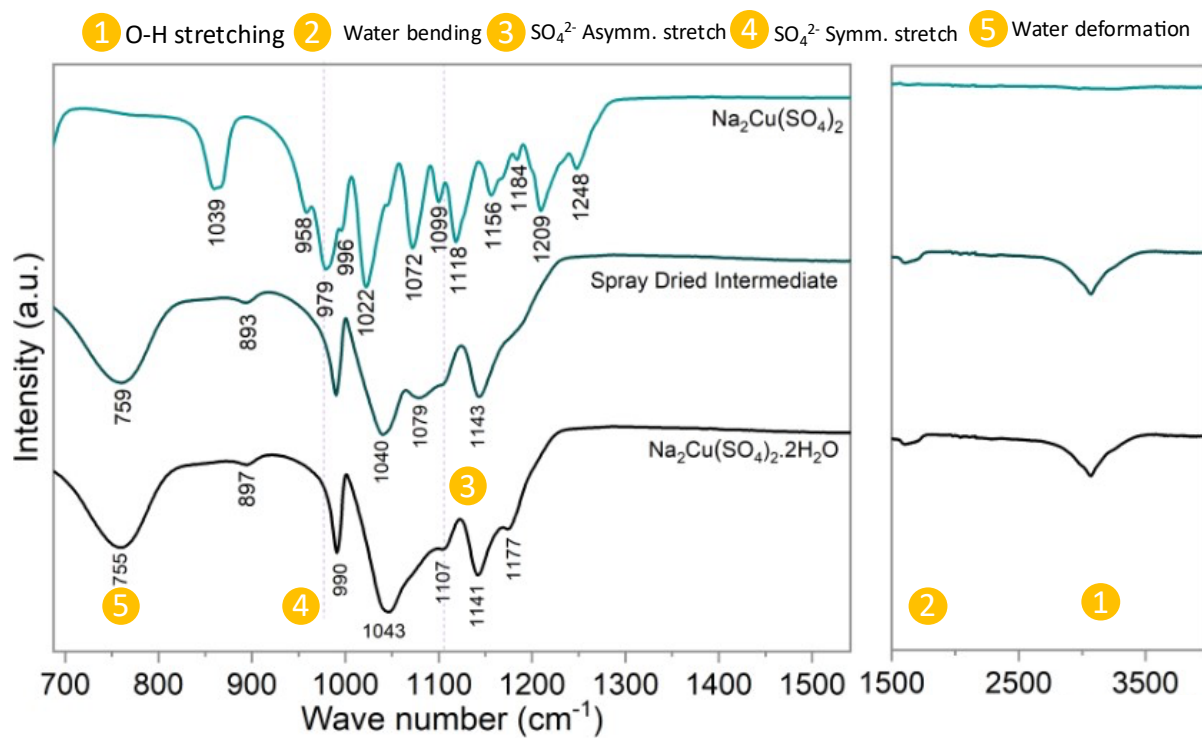


Fig. S3 FTIR spectra, acquired in ATR mode, of the Cu-krh, src and spray dried intermediate powder. The spectra of Cu-krh and spray dried intermediate powder are quite similar. However, the XRD patterns, as shown in figure 1, are different.

Table S3. Bader charge analysis during removal of one sodium from src $\text{Na}_2\text{Cu}(\text{SO}_4)_2$.

Atoms in full-sodiated phase	Bader Charge (Δq)	Atoms in half-desodiated phase	Bader charge (Δq)
Na1			
Na2	+0.8568	Na2	+0.8657
Na3	+0.8526	-	
Na4	+0.8526	Na4	+0.8578
Na5	+0.8461	Na5	+0.8461
Na6	+0.8461	-	
Na7	+0.8551	Na7	+0.8549
Na8	+0.8551	-	
Na9	+0.8639	Na9	+0.8638
Na10	+0.8639	-	
Na11	+0.8502	Na11	+0.8529
Na12	+0.8502	-	
Na13	+0.8483	Na13	+0.8490
Na14	+0.8483	-	
Na15	+0.8431	-	
Na16	+0.8431	Na16	+0.8459

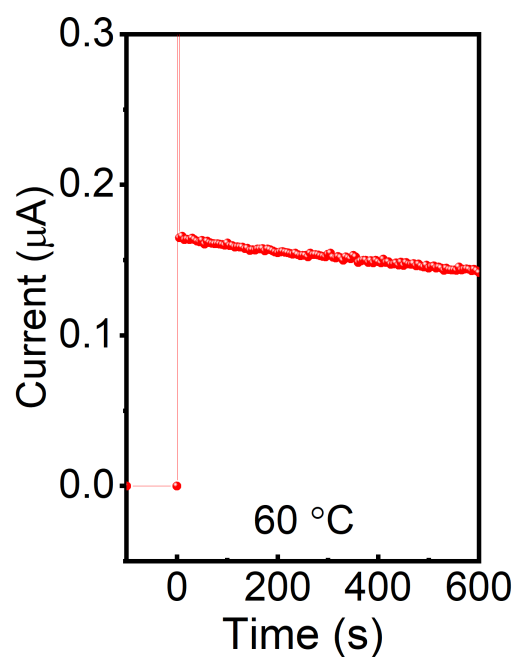


Fig. S4 The current response of Cu-krh acquired during potentiostatic polarization under an applied potential step of 2V at 60 °C.

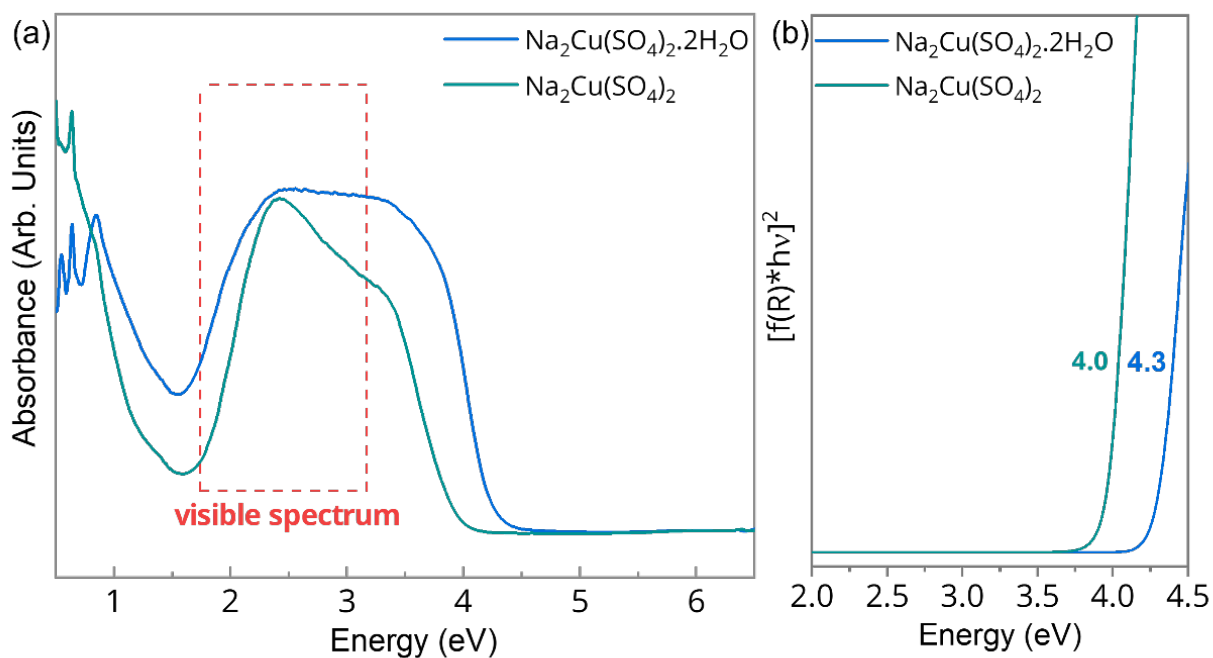


Fig. S5 (a) UV-VIS-NIR absorption spectra of the src and Cu-krh compounds, and (b) Optical band gap for the src and Cu-krh calculated using Kubelka-Munk function ($n = 2$) applied to UV-VIS-NIR spectra

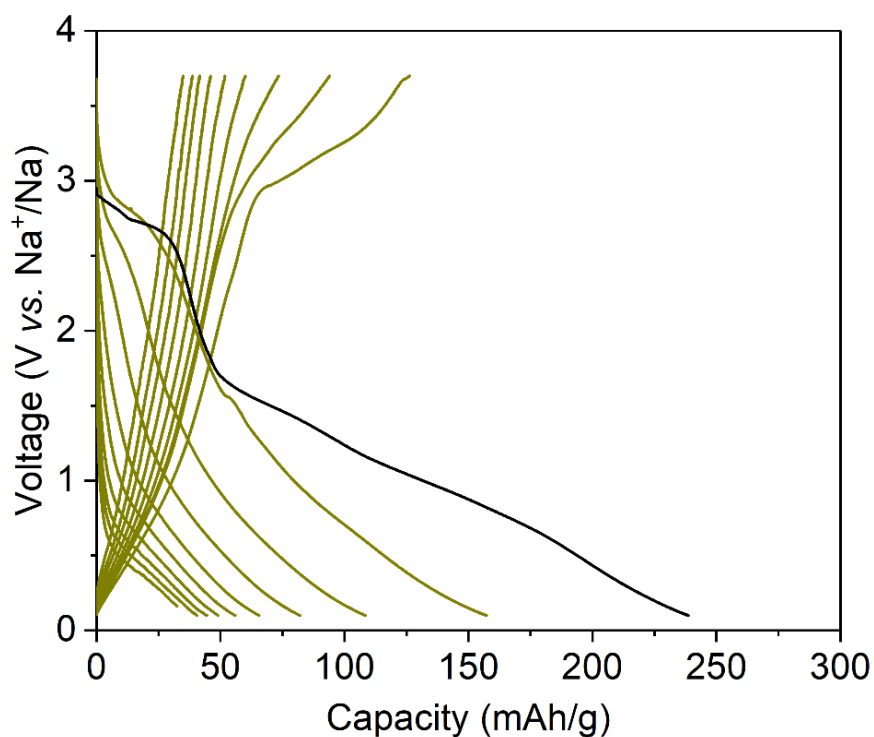


Fig. S6 Galvanostatic profile of Cu-src $\text{Na}_2\text{Cu}(\text{SO}_4)_2$ acquired at a current rate of 2 mA/g using 1M NaPF_6 - EC/DEC electrolyte and Na metal anode in half cell. The black and dark yellow color represent the first and subsequent cycles during the galvanostatic cycling.

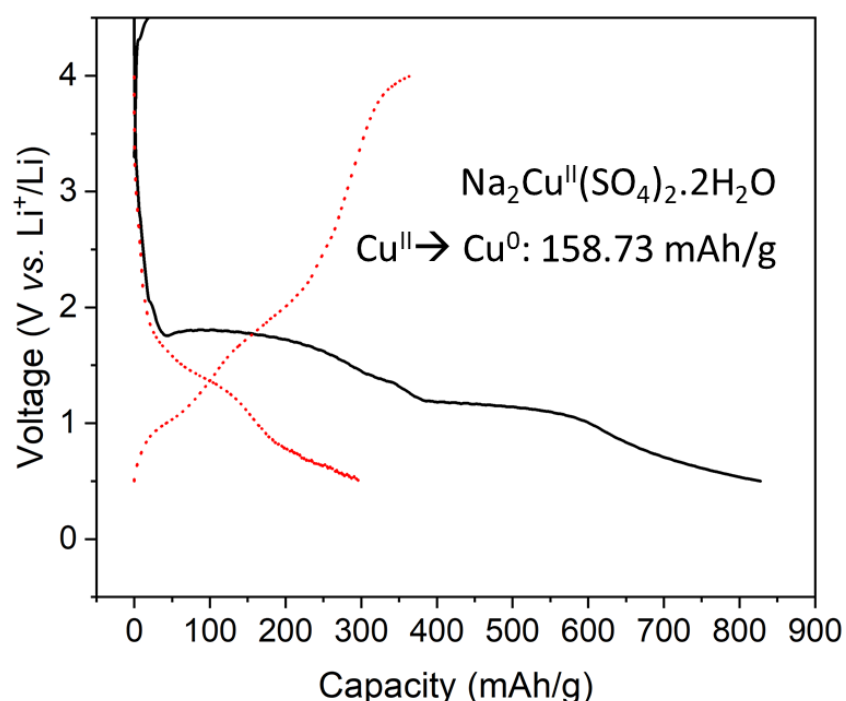


Fig. S7 Galvanostatic profile of Cu-krh $\text{Na}_2\text{Cu}(\text{SO}_4)_2 \cdot 2\text{H}_2\text{O}$ acquired at a current rate of 2 mA/g using 1M LiClO_4 -PC electrolyte and Li metal anode in half cell. The black and red line represent the first and second cycle during the galvanostatic cycling. A different galvanostatic profile of Cu-krh from src may stem from different structure and the water of hydration¹. The in-depth mechanistic understanding will be pursued in future.

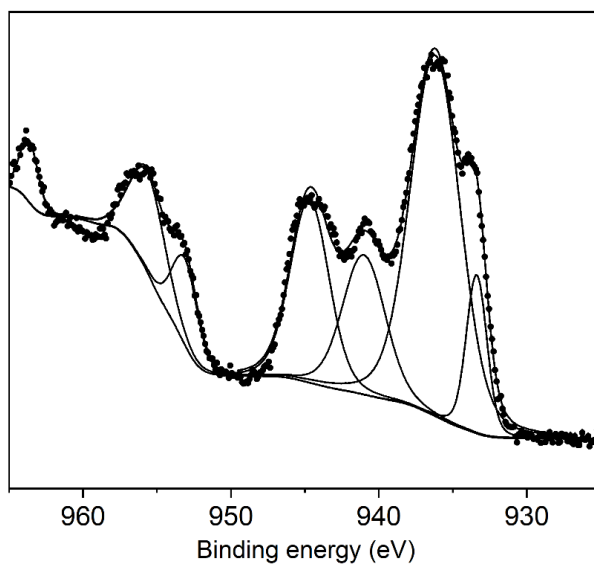


Fig. S8 XPS spectrum of Cu 2p core peak for pristine Cu-krh electrode. The characteristic satellite peaks of Cu^{2+} can be seen at the binding energies: 941.01 eV, 944.68 eV and 963.65 eV.

References

1. Schwieger, J. N.; Kraytsberg, A.; Ein-Eli, Y. Copper Sulfates as Cathode Materials for Li Batteries. *J. Power Sources* **2011**, *196* (3), 1461–1468. <https://doi.org/10.1016/j.jpowsour.2010.07.090>.